Supporting Information

Steering the Electronic Communication between Al/Ru Bimetallic Clusters in Metal–Organic Frameworks Composite for Accelerating Hydrogen Evolution Kinetics

Xueting Song [a], Haifeng Yang [a], Chenghua Zhang [b, *], Guizhi Zhang [a], Hong Wu [a], Youzhou He [a], Min Fu [a], Xingyan Liu [a, *], Siqi Li [d], Siping Wei [c, *]

[a] *Chongqing Key Laboratory of Catalysis and New Environmental Materials, College of Environment and Resources, Chongqing Technology and Business University, Chongqing 400067, China.*

[b] *School of Pharmacy, North Sichuan Medical College, Nanchong 637100, China.*

[c] *Central Nervous System Drug Key Laboratory of Sichuan Province, Department of Medicinal Chemistry, School of Pharmacy, Southwest Medical University, Luzhou 646000, China.*

[d] *State Key Joint Laboratory of Environment Simulation and Pollution Control, School of Environment, Tsinghua University, Beijing 100084, China.*

[*] *E-mail addresses: xyliuctbu@126.com (X. Liu), zchua@nsmc.edu.cn (C. Zhang), swei1225@swmu.edu.cn (S. Wei)*

Synthesis of 5,10,15,20-tetra (4-methoxycarbonylphenyl) porphyrin (TMCPP)

Firstly, methyl 4-formylbenzoate (0.086 mol, 14.410 g) was completely dissolved in propionic acid (250 mL), then pyrrole solution (6.1 mL pyrrole and 20 mL propionic acid) was added slowly, and then the mixture was refluxed at 150 °C for 12 h. After the reaction was stopped, the precipitate was obtained by suction filtration, and washed with a large amount of EtOH, ethyl acetate and a small amount of THF respectively. The precipitate was dried at 70 °C for 12 h to obtain the purple product, recorded as TMCPP.

Synthesis of 5,10,15,20-tetrakis (4-carboxyphenyl) porphyrin (TCPP)

TMCPP (0.600 g) was dissolved in 24 mL (V_{THF}: V_{MeOH} =1:1) mixture, then KOH (2.88 mol/L) aqueous solution was added to it and reflux was conducted at 90 °C for 12 h. After the mixed solution was cooled, the organic solvent was removed by the rotary evaporation method, and then the pH of the solution was adjusted with 0.1 M HCl to make pH=2 and the solid product was precipitated. Finally, the solid product was washed several times with water and dried at 80 °C to obtain the target product, recorded as TCPP.

Synthesis of Al_x/Ru_y-TCPP with different molar ratios

To synthesize Al_x/Ru_y-TCPP (x = 0.45, 0.4, 0.35, 0.3, 0.25 mmol, and y = 0.05, 0.1, 0.15, 0.2, 0.25 mmol), $AlCl_3 \cdot 6H_2O$ (109, 97, 85, 73, 61 mg), $RuCl_3 \cdot xH_2O$ (10.5, 21, 31, 42, 52 mg) and TCPP (161 mg) were added in 20 mL deionized water, respectively. And the ultrasonic homogeneous mixture was placed in a 50 mL high-pressure reactor at 180 ℃ for 16 h.

Characterization

The phase purity and crystal structure of as-prepared catalysts were characterized by X-ray powder diffraction (XRD) patterns (XPD-6100, Shimadzu, Japan); The morphology of as-prepared catalysts was characterized by scanning electron microscopy (SEM) micrographs (Zeiss Merlin, Germany); Energy dispersive X-Ray spectroscopy (EDX) (FEI Quanta 650FEG, USA) was conducted to determine the elemental composition of the composite material; The chemical states of various elements in the material were studied by X-ray photoelectron spectroscopy (XPS) (Thermo Scientific K-Alpha, USA); Ultraviolet-visible diffuse reflectance spectroscopy (UV-vis DRS, Shimadzu, Japan) of all materials are obtained in the range of 300~800 nm; Fourier transform infrared (FT-IR) spectra were recorded in the range of 400–4000 cm^{-1} with a IRPrestige-21 (Shimadzu, Japan) spectrophotometer; Based on Brunauer-Emmett-Teller (BET) measurements (ASAP 2020, USA), the specific surface area of the materials was determined using N_2 adsorption/desorption isotherms, and the pore volumes were obtained using the Barrett-Joyner-Halenda (BJH) method.

Electrochemical measurements

All electrochemical tests all catalysts were carried out on a CHI660E electrochemical workstation (Chenhua Co., LTD., Shanghai, China). A standard three-electrode cell was used, with a glassy carbon electrode as the working electrode, a saturated calomel electrode as the reference electrode, and a graphite rod as the counter electrode. Typically, 5 mg of sample was uniformly dispersed by sonication in a mixed solution (490 μL of deionized water, 490 μL of absolute ethanol and 20 μL

of 5 wt% Nafion). Then, 5 μL of the above solution was dropped on a glassy carbon electrode with a diameter of 3 mm and dried at room temperature as a working electrode. The mass loading was 0.35 mg·cm^{-2} in 0.5 M H_2SO_4 and the commercial 20 wt% Pt/C electrode was also prepared using the same procedure for comparison.

HER tests

The linear scanning voltammograms (LSV) were tested in a 0.5 M H_2SO_4 solution under the potential range from 0 to -1 V and the scan rate of 5 mV·s^{-1}. All the potential values provided were reported relative to RHE and measured relative to the SCE electrode according to *E* (*vs*. RHE) = *E* (*vs.* SCE) + 0.241 + 0.0592 × pH. EIS was obtained by a frequency range from 100 k to 0.1 Hz with an overpotential of -0.3 V versus RHE. Cyclic voltammetry (CV) was tested at different scan rates (20, 40, 60, 80, 100, 120, 140, 160, 180 and 200 mV·s^{-1}) in a potential window (0.141-0.541 V *vs*. RHE) where no Faradaic process occurs. The electrochemically active surface area was evaluated from double-layer capacitance (C_{dl}). Stability test through cyclic potential scanning and chronoamperometry method (constant density of 10 mA·cm^{-2} current density).

Calculation Methods

We have employed the first-principles [1,2] to perform all density functional theory (DFT) calculations within the generalized gradient approximation (GGA) using the Perdew-Burke-Ernzerhof (PBE) [3] formulation. We have chosen the projected augmented wave (PAW) potentials [4,5] to describe the ionic cores and take valence electrons into account using a plane wave basis set with a kinetic energy cutoff of

520 eV. Partial occupancies of the Kohn−Sham orbitals were allowed using the Gaussian smearing method and a width of 0.05 eV. The electronic energy was considered self-consistent when the energy change was smaller than 10^{-5} eV. A geometry optimization was considered convergent when the energy change was smaller than 0.03 eV $Å^{-1}$. The vacuum spacing in a direction perpendicular to the plane of the structure is 20 Å for the MOFs surface. The Brillouin zone integration is performed using 1×1×1 Monkhorst-Pack k-point sampling for a structure. Finally, the adsorption energies (Eads) were calculated as Eads = Ead/sub - Ead - Esub, where Ead/sub, Ead, and Esub are the total energies of the optimized adsorbate/substrate system, the adsorbate in the structure, and the clean substrate, respectively. The free energy was calculated using the equation:

$$G=E+ZPE-TS$$

where G, E, ZPE and TS are the free energy, total energy from DFT calculations, zero-point energy and entropic contributions, respectively.

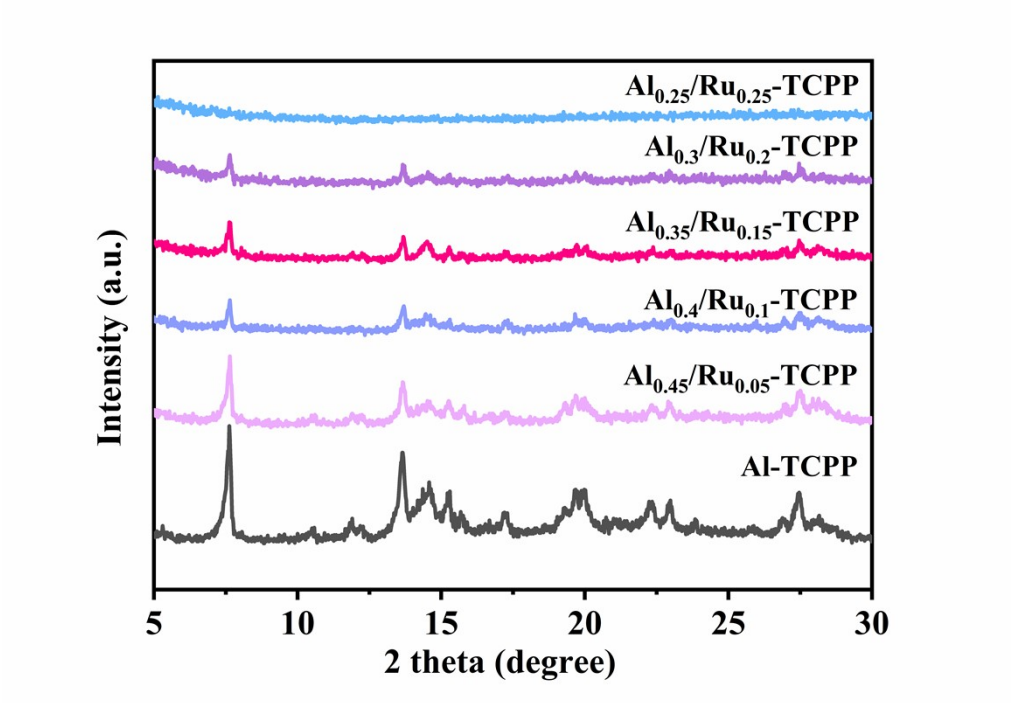

Fig. S1. XRD of Al-TCPP, Ru-TCPP and Al_x/Ru_y-TCPP prepared with different molar ratios (x = 0.25, 0.3, 0.35, 0.4, 0.45, and y = 0.25, 0.2, 0.15, 0.1, 0.05).

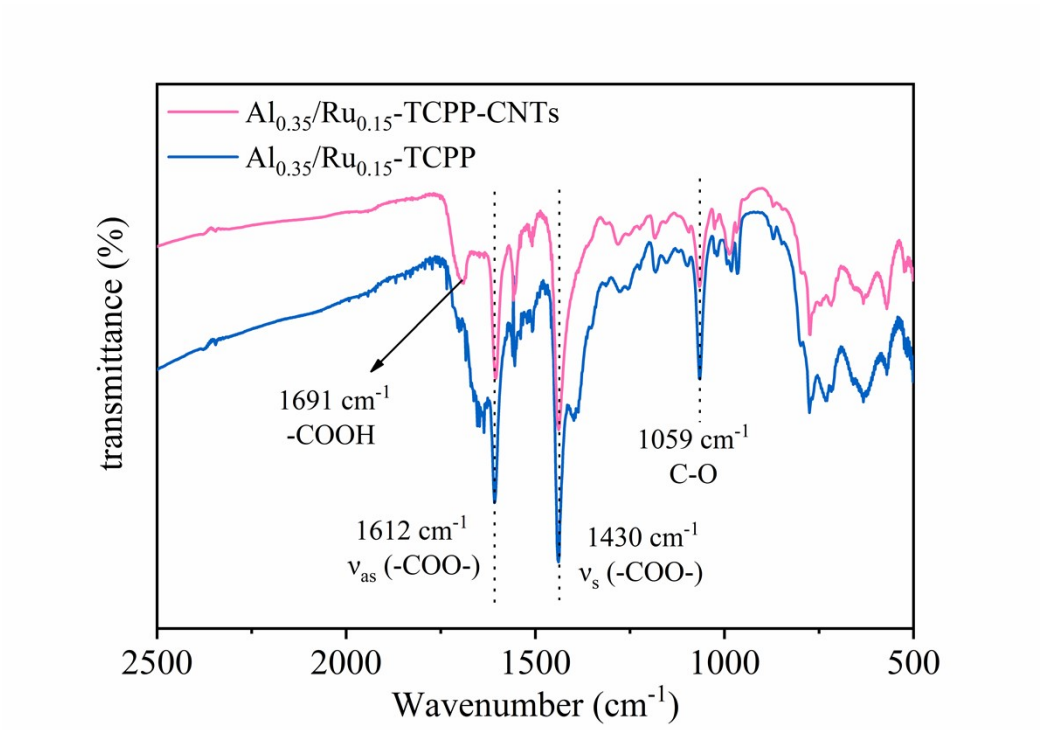

Fig. S2. FT-IR spectra of $Al_{0.35}/Ru_{0.15}$-TCPP and $Al_{0.35}/Ru_{0.15}$-TCPP-CNTs.

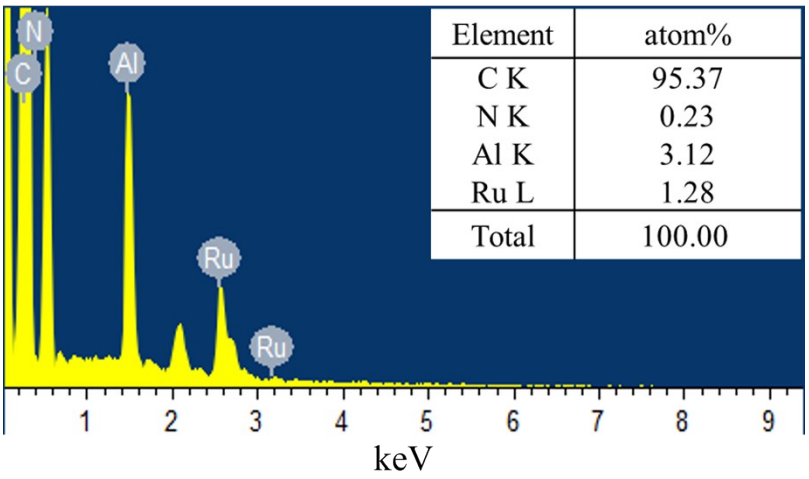

Element	atom%
C K	95.37
N K	0.23
Al K	3.12
Ru L	1.28
Total	100.00

Fig. S3. EDS spectra and atomic ratio of $Al_{0.35}/Ru_{0.15}$-TCPP-CNTs.

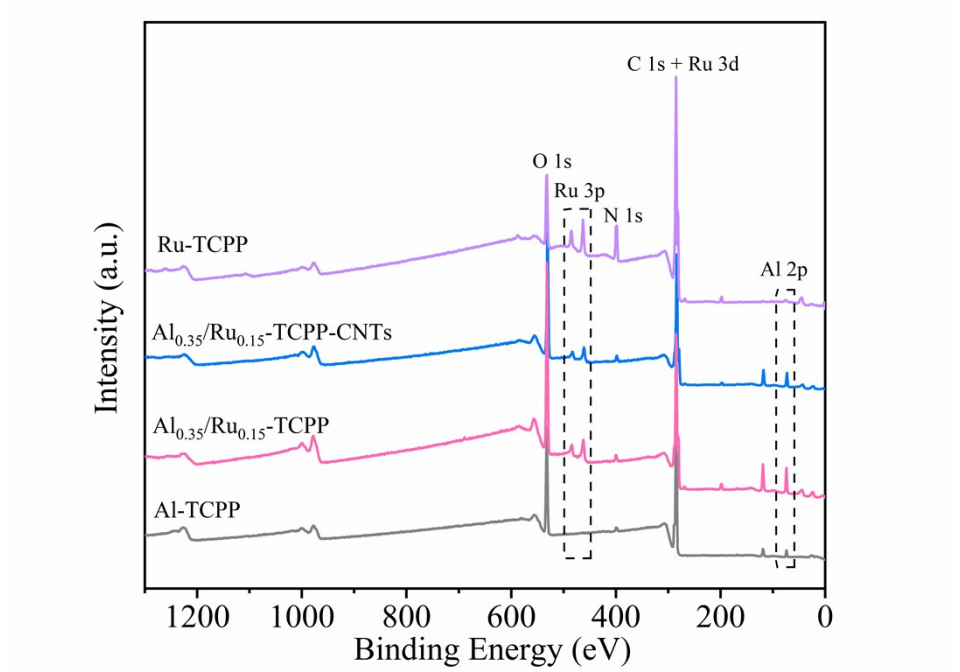

Fig. S4. XPS full spectra of Al-TCPP, $Al_{0.35}/Ru_{0.15}$-TCPP, $Al_{0.35}/Ru_{0.15}$-TCPP-CNTs and Ru-TCPP.

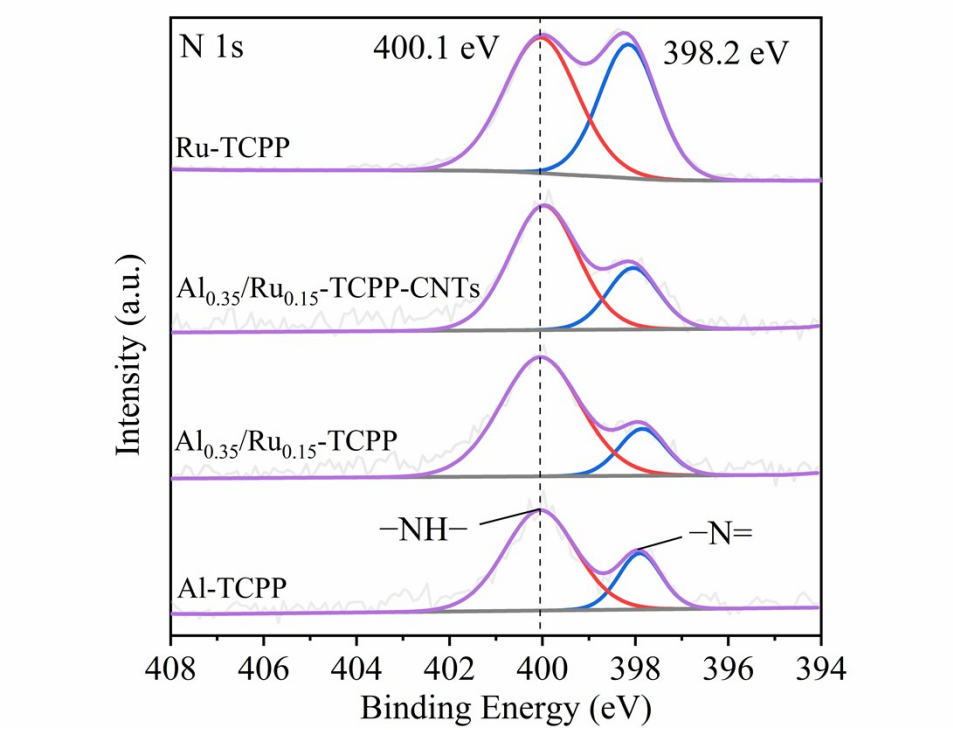

Fig. S5. N1s spectra of Al-TCPP, $Al_{0.35}/Ru_{0.15}$-TCPP, $Al_{0.35}/Ru_{0.15}$-TCPP-CNTs and Ru-TCPP.

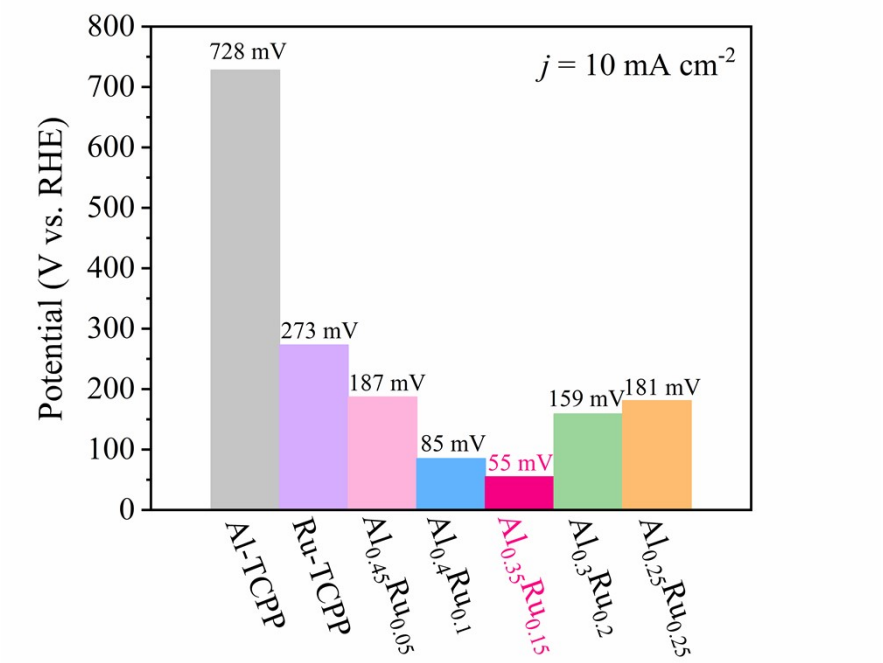

Fig. S6. Comparison of overpotentials at 10 $mA \cdot cm^{-2}$ for different proportions of Al_x/Ru_y-TCPP.

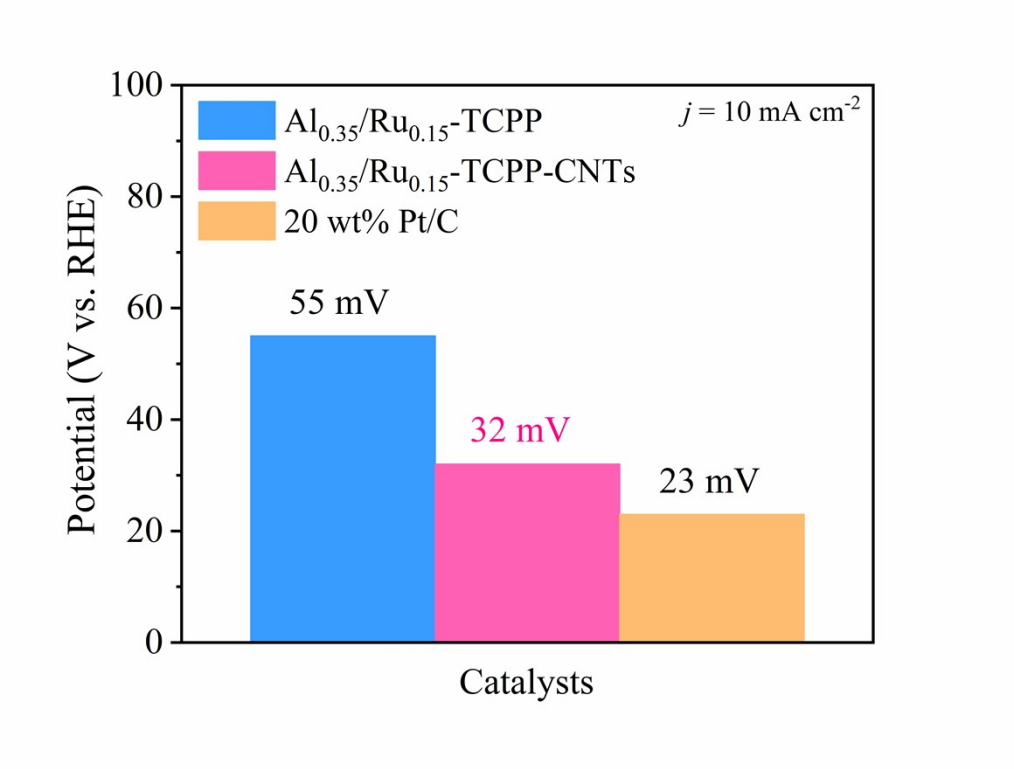

Fig. S7. Corresponding overpotentials of $Al_{0.35}/Ru_{0.15}$-TCPP-CNTs, $Al_{0.35}/Ru_{0.15}$-TCPP and 20 wt% Pt/C (at 10 mA·cm^{-2}).

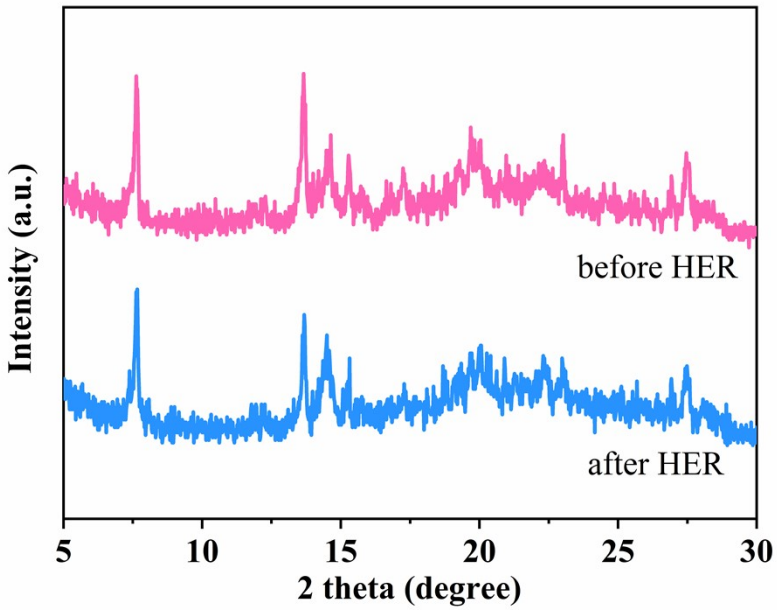

Fig. S8. XRD patterns of $Al_{0.35}/Ru_{0.15}$-TCPP-CNTs before and after long-term stability testing in 0.5 M H_2SO_4.

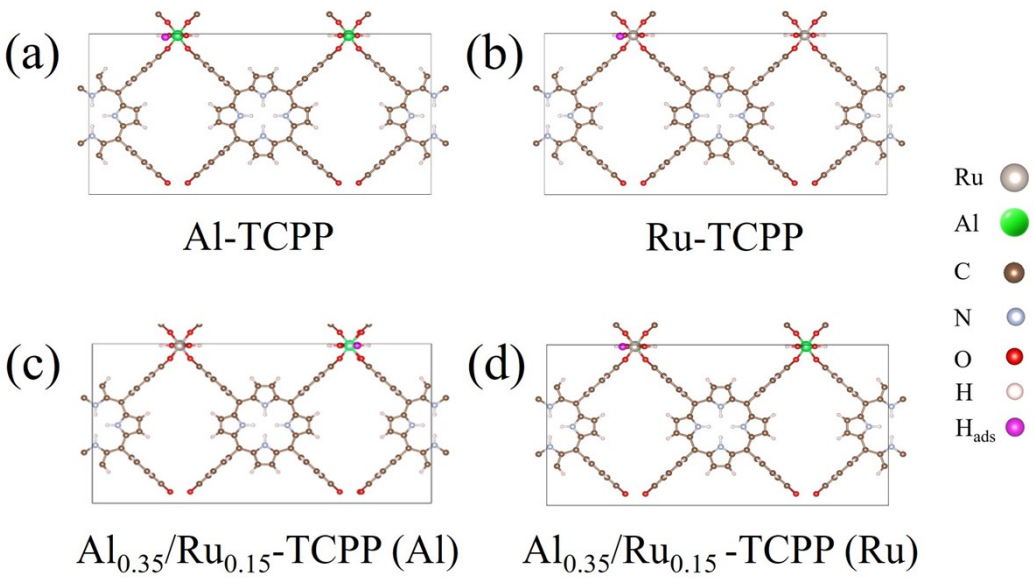

Fig. S9. (d) H-adsorption structures of the Al and Ru sites of Al-TCPP, Ru-TCPP, and $Al_{0.35}/Ru_{0.15}$-TCPP.

Table S1. Structural parameters of different samples.

Sample	S_{BET} ($m^2 \cdot g^{-1}$)	Total Pore Volume ($cm \cdot g^{-1}$)	Pore Size (nm)
$Al_{0.35}/Ru_{0.15}$-TCPP	220.55	0.252	5.7
$Al_{0.35}/Ru_{0.15}$-TCPP-CNTs	440.41	0.321	15.2

Table S2. Parameters from peak deconvolution of XPS spectra in the C 1s region.

Binding Energy (eV)	C=O	C-N	C-C/C=C
Al-TCPP	288.78	286.63	284.79
$Al_{0.35}/Ru_{0.15}$-TCPP	289.13	286.55	284.82
$Al_{0.35}/Ru_{0.15}$-TCPP-CNTs	289.22	286.71	284.81
Ru-TCPP	288.82	286.54	284.80

Table S3. Parameters from peak deconvolution of XPS spectra in the Ru 3d region.

Binding Energy (eV)	Ru $3d_{3/2}$	Ru $3d_{5/2}$
Al-TCPP	-	-
$Al_{0.35}/Ru_{0.15}$-TCPP	285.24	-
$Al_{0.35}/Ru_{0.15}$-TCPP-CNTs	285.55	-
Ru-TCPP	285.58	281.86

Table S4. Parameters from peak deconvolution of XPS spectra in the O 1s region.

Binding Energy (eV)	O-H	O-C=O	Al-O	Ru-O
Al-TCPP	533.35	531.95	530.66	-
$Al_{0.35}/Ru_{0.15}$-TCPP	533.19	532.12	531.11	530.14
$Al_{0.35}/Ru_{0.15}$-TCPP-CNTs	533.42	532.29	531.11	530.14
Ru-TCPP	533.23	531.81	-	530.68

Table S5. Parameters from peak deconvolution of XPS spectra in the Al 2p region.

Binding Energy (eV)	Al 2p
Al-TCPP	74.16
$Al_{0.35}/Ru_{0.15}$-TCPP	74.47
$Al_{0.35}/Ru_{0.15}$-TCPP-CNTs	74.57

Table S6. Parameters from peak deconvolution of XPS spectra in the Ru 3p region.

Binding Energy (eV)	Ru $3p_{1/2}$	Ru $3p_{1/2}$	Ru $3p_{3/2}$	Ru $3p_{3/2}$
Ru-TCPP	488.96	485.03	465.98	462.79
$Al_{0.35}/Ru_{0.15}$-TCPP	488.56	484.47	465.68	462.16
$Al_{0.35}/Ru_{0.15}$-TCPP-CNTs	487.77	484.21	465.44	461.93

Table S7. Elemental compositions (atom%) of $Al_{0.35}/Ru_{0.15}$-TCPP-CNTs obtained from the XPS results.

Catalysts	Al	Ru	C	N	O	Al/Ru
$Al_{0.35}/Ru_{0.15}$-TCPP	13.71	5.67	46.03	2.15	32.44	2.42
$Al_{0.35}/Ru_{0.15}$-TCPP-CNTs	9.91	4.29	54.88	2.61	28.31	2.31

Table S8. The HER activities of the $Al_{0.35}/Ru_{0.15}$-TCPP-CNTs compared with other recently reported catalysts in 0.5 M H_2SO_4.

Catalysts	*At 10 mA cm^{-2}* (in 0.5 M H_2SO_4)	References
$Al_{0.35}/Ru_{0.15}$-TCPP-CNTs	32 mV	Our work
$Al_{0.35}/Ru_{0.15}$-TCPP	55 mV	Our work
$RuRh_2$	34 mV	*Adv. Sci.* [6]
Ru-$WO_{2.72}$	40 mV	*Appl. Catal. B.* [7]
$Co_{1-x}Ru_x$/GC	44 mV	*Chem. Eng. J.* [8]
Ru@$Ti_3C_2T_x$-NS	46.75 mV	*Int. J. Hydrogen Energy.* [9]
RuMo-Ar	48 mV	*Small Struct.* [10]
Ru_1CoP/CDs	49 mV	*Angew. Chem. Int. Ed.* [11]
RuP_2/CNT	58 mV	*Chem. Eur. J.* [12]
Ru@B–$Ti_3C_2T_x$	62.9 mV	*Small* [13]
ECM@Ru	63 mV	*Adv. Energy Mater.* [14]
Ru_{SA}-N-S-$Ti_3C_2T_x$	76 mV	*Adv. Mater.* [15]
RuP_2@PC	77.2 mV	*J. Mater. Chem. A* [16]
Ru_3Al	79 mV	*Inorg. Chem.* [17]
RuNi/CFC	80.2 mV	*Nanoscale* [18]
MoP-Ru_2P/NPC	82 mV	*Appl. Catal. B.* [19]
Ru/Ni_2P@NPC	89 mV	*ACS Sustain. Chem. Eng.* [20]
Ru@Co/N-CNTs	92 mV	*ACS Sustain. Chem. Eng.* [21]
Ru@N-TiO_2/C	116 mV	*J. Mater. Chem. A* [22]

References

1 G. Kresse and J. Furthmüller, *Comput Mater Sci*, 1996, **6**, 15–50.

2 G. Kresse and J. Furthmüller, *Phys Rev B Condens Matter Mater Phys*, 1996, **54**, 11169–11186.

3 J. P. Perdew, K. Burke and M. Ernzerhof, *Phys Rev Lett*, 1996, **77**, 3865–3868.

4 D. Joubert, *Phys Rev B Condens Matter Mater Phys*, 1999, **59**, 1758–1775.

5 P. E. Blöchl, *Phys Rev B*, 1994, **50**, 17953–17979.

6 X. Mu, J. Gu, F. Feng, Z. Xiao, C. Chen, S. Liu and S. Mu, *Advanced Science*, 2021, **8**, 2002341.

7 L. Peng, L. Su, X. Yu, R. Wang, X. Cui, H. Tian, S. Cao, B. Y. Xia and J. Shi, *Appl Catal B*, 2022, **308**, 121229.

8 S. Zhang, Y. Rui, X. Zhang, R. Sa, F. Zhou, R. Wang and X. Li, *Chemical Engineering Journal*, 2021, **417**, 128047.

9 Y. Yang, Z. Yu, X. An, X. Duan, M. Chen, J. Zhang, X. Hao, A. Abudula and G. Guan, *Int J Hydrogen Energy*, 2023, **48**, 9163–9171.

10 C. Li, J. Chen, K. C. Chong, L. Wang and B. Liu, *Small Struct*, 2023, 2300394.

11 H. Song, M. Wu, Z. Tang, J. S. Tse, B. Yang and S. Lu, *Angewandte Chemie - International Edition*, 2021, **60**, 7234–7244.

12 M. Cheng, H. Geng, Y. Yang, Y. Zhang and C. C. Li, *Chemistry - A European Journal*, 2019, **25**, 8579–8584.

13 M. Bat-Erdene, M. Batmunkh, B. Sainbileg, M. Hayashi, A. S. R. Bati, J. Qin, H. Zhao, Y. L. Zhong and J. G. Shapter, *Small*, 2021, **17**, 2102218.

14 H. Zhang, W. Zhou, X. F. Lu, T. Chen and X. W. Lou, *Adv Energy Mater*, 2020, **10**, 2000882.

15 V. Ramalingam, P. Varadhan, H. C. Fu, H. Kim, D. Zhang, S. Chen, L. Song, D. Ma, Y. Wang, H. N. Alshareef and J. H. He, *Advanced Materials*, 2019, **31**, 1903841.

16 J. Sen Li, M. J. Huang, Y. W. Zhou, X. N. Chen, S. Yang, J. Y. Zhu, G. D. Liu, L. J. Ma, S. H. Cai and J. Y. Han, *J Mater Chem A Mater*, 2021, **9**, 12276–12282.

17 H. Zhang, Q. Liu, J. Xu, L. Wei, Q. Liu and X. Kong, *Inorg Chem*, 2019, **58**, 8267–8270.

18 M. Yuan, C. Wang, Y. Wang, Y. Wang, X. Wang and Y. Du, *Nanoscale*, 2021, **13**, 13042–13047.

19 Y. Gao, Z. Chen, Y. Zhao, W. Yu, X. Jiang, M. He, Z. Li, T. Ma, Z. Wu and L. Wang, *Appl Catal B*, 2022, **303**, 120879.

20 J. Q. Chi, X. Y. Zhang, X. Ma, B. Dong, J. Q. Zhang, B. Y. Guo, M. Yang, L. Wang, Y. M. Chai and C. Liu, *ACS Sustain Chem Eng*, 2019, **7**, 17714–17722.

21 Z. Liu, X. Yang, G. Hu and L. Feng, *ACS Sustain Chem Eng*, 2020, **8**, 9136–9144.

22 W. Xu, H. Xie, F. Cao, S. Ran, Y. Duan, B. Li and L. Wang, *J Mater Chem A Mater*, 2022, **10**, 23751-23759.